Glycosylation controls sodium-calcium exchanger 3 sub-cellular localization during cell cycle

Tong Liu, Jian Zhao, Cristian Ibarra, Maxime Garcia, Per Uhlén, Monica Nistér

European Journal of Cell Biology 97 (2018) 190–203

Contents lists available at ScienceDirect

European Journal of Cell Biology

journal homepage: www.elsevier.com/locate/ejcb

Glycosylation controls sodium-calcium exchanger 3 sub-cellular localization during cell cycle

Tong Liu[a], Jian Zhao[a,*], Cristian Ibarra[b], Maxime U. Garcia[a], Per Uhlén[b], Monica Nistér[a,*]

[a] Department of Oncology-Pathology, Karolinska Institutet, CCK R8:05, Karolinska University Hospital Solna, SE-171 76 Stockholm, Sweden
[b] Department of Medical Biochemistry and Biophysics, Karolinska Institutet, SE-171 77 Stockholm, Sweden

ARTICLE INFO

Keywords:
Na^+/Ca^{2+} exchanger
N-linked glycosylation
Cell cycle
Cell proliferation
Subcellular localization
ER

ABSTRACT

The Na^+/Ca^{2+} exchanger (NCX) is a membrane antiporter that has been identified in the plasma membrane, the inner membrane of the nuclear envelope and in the membrane of the endoplasmic reticulum (ER). In humans, three genes have been identified, encoding unique NCX proteins. Although extensively studied, the NCX's sub-cellular localization and mechanisms regulating the activity of different subtypes are still ambiguous. Here we investigated the subcellular localization of the NCX subtype 3 (NCX3) and its impact on the cell cycle. Two phenotypes, switching from one to the other during the cell cycle, were detected. One phenotype was NCX3 in the plasma membrane during S and M phase, and the other was NCX3 in the ER membrane during resting and interphase. Glycosylation of NCX3 at the N45 site was required for targeting the protein to the plasma membrane, and the N45 site functioned as an on-off switch for the translocation of NCX3 to either the plasma membrane or the membrane of the ER. Introduction of an *N*-glycosylation deficient NCX3 mutant led to an arrest of cells in the G0/G1 phase of the cell cycle. This was accompanied by accumulation of de-glycosylated NCX3 in the cytosol (that is in the ER), where it transported calcium ions (Ca^{2+}) from the cytosol to the ER. These results, obtained in transfected HEK293T and HeLa and confirmed endogenously in SH-SY5Y cells, suggest that cells can use a dynamic Ca^{2+} signaling toolkit in which the NCX3 sub-cellular localization changes in synchrony with the cell cycle.

1. Introduction

The calcium ion (Ca^{2+}) is an intracellular second messenger that plays a crucial role in many biological processes (Berridge et al., 2000). The basal cytosolic concentration of Ca^{2+} is low (100 nM) and an accurate control of the Ca^{2+} homeostasis is essential for cell life, since a high level of Ca^{2+} is toxic to the cell. This is mainly accomplished by a variety of Ca^{2+}-ATPases (the plasma membrane Ca^{2+} pump (PMCA) and sarco/endo-plasmic reticulum Ca^{2+}-ATPases (SERCA)), the mitochondrial Ca^{2+} uniporter, and the Na^+/Ca^{2+} exchanger (NCX) (Hilge et al., 2006; Uhlen and Fritz, 2010).

NCX, as a plasma membrane antiporter, is important for modulating the intracellular Ca^{2+} homeostasis by coupling Ca^{2+} efflux to Na^+ influx (forward mode) and Na^+ efflux to Ca^{2+} influx (reverse mode), depending on the transmembrane ion gradient and membrane potential (Iwamoto, 2007). The NCX has also been found in the inner membrane of the nuclear envelope (NE), where it is proposed to regulate Ca^{2+} flux between the nucleoplasm and the NE (Xie et al., 2002; Wu et al., 2009; Brini and Carafoli, 2011). In mammals, three NCX subtypes have been reported: NCX1 (Nicoll et al., 1990), NCX2 (Li et al., 1994), and NCX3 (Nicoll et al., 1996). They share ~70% sequence identity and show few functional differences (Iwamoto and Shigekawa, 1998; Linck et al., 1998; Hilge et al., 2006).

The NCX protein contains a cleaved signal sequence, a short glycosylated extracellular region (Hryshko et al., 1993), eleven transmembrane segments (TMS), and a large central cytoplasmic loop. The eleven TMSs can be grouped into an N-terminal hydrophobic domain, composed of the first five TMSs (1–5), and a C-terminal hydrophobic domain, composed of the last six TMSs (6–11). Two highly conserved regions, named alpha-1 and −2 repeats were identified in the protein (Schwarz and Benzer, 1997; Liao et al., 2012) and suggested to be involved in the Na^+ and Ca^{2+} binding (Iwamoto et al., 1999; Liao et al., 2012). The N-terminal hydrophobic domain is separated from the C-terminal hydrophobic domain through a large hydrophilic intracellular loop (Nicoll et al., 1999). Removal or cleavage of the loop results in an hyperactive exchanger and calcium refilling of the ER (Matsuoka et al., 1993; Michel et al., 2017). The exchanger inhibitory peptide (XIP) locates in the N-terminus of this loop, and the Ca^{2+} binding domains

* Corresponding authors.
E-mail addresses: Jian.Zhao@ki.se (J. Zhao), Monica.Nister@ki.se (M. Nistér).

https://doi.org/10.1016/j.ejcb.2018.02.004
Received 15 May 2017; Received in revised form 13 August 2017; Accepted 27 February 2018

CBD1 and CBD2 plus an α-catenin-like domain constitute the Ca^{2+} binding function of the loop. CBD1 is the main sensor of calcium content and activates the exchanger in a Ca^{2+} transient state (Hilge et al., 2006), whereas the inactivation of NCX is regulated by CBD2 (Giladi and Khananshvili, 2013).

Glycosylation is a ubiquitous post-translational modification of proteins in animal systems playing a number of crucial roles from protein folding and quality control to biological recognition events (Moremen et al., 2012). It has been described that protein *N*-glycosylation plays a crucial role in controlling the number of voltage-gated calcium channels embedded in the plasma membrane and also in their functional gating properties (Lazniewska and Weiss, 2017). Although the NCX3 protein, as the key player in cytosolic calcium extrusion, has been localized at the junction of PM and ER/SR, the sub-cellular localization and trafficking of the NCX3 proteins have still not been described in detail.

In this study, we show that, in mammalian cells, the sub-cellular localization of the NCX3 protein varies between resting/interphase cells and cells in the cell cycle. Firstly, we can identify two primary phenotypes. One is NCX3 localized in the plasma membrane (NCX3-PM), the other is NCX3 distributed in the cytoplasm (NCX3-ER). Secondly, in interphase cells, NCX3 localizes to the ER and nuclear membrane, while during S-phase, mitosis and cell division it is observed in the plasma membrane. Intriguingly, the presence and role of *N*-glycosylation of human NCX3 has not previously been defined. Here we show that modification of NCX3 by *N*-linked glycosylation at a single asparagine residue, N45, is required for targeting of the protein to the plasma membrane. Importantly, this mechanism also affects cells' progression through the cell cycle.

2. Materials and methods

2.1. Cell culture and transfection

HEK293T cells were grown in Dulbecco's modified Eagle's media (Thermo Fisher), supplemented with 10% fetal bovine serum and 1% Pen/Strep (Thermo Fisher). HeLa cells were grown in Eagle's Minimum Essential Medium (Thermo Fisher), supplemented with fetal bovine serum to a final concentration of 10%. Transient transfections with different plasmids were carried out using Lipofectamine Plus or Lipofectamine 2000 according to the manufacturer's instructions (Thermo Fisher). Stable expression cell lines were established following the protocol from Thermo Fisher.

2.2. Construction of plasmids and site-directed mutagenesis

The cDNA containing the entire open reading frame (ORF) of the human NCX3.2 isoform had previously been cloned into the pcDNA3.1 expression plasmid (Lindgren et al., 2005), generating a fusion of NCX3 cDNA with a C-terminal V5-His tag (pcDNA3.1-NCX3.2/V5-His). The plasmids pcDNA3.1-GFP and pcDNA3.1/V5-His were used as control plasmids.

The recombinant NCX3.2-EmGFP was attained by polymerase chain reaction (PCR). The EmGFP fragment was amplified by PCR using primers SP + GFP-F: 5′-GCT GGT GGC TCA GGG GAC ATG GTG AGC AAG −3′ and GFP + NCX3-R: 5′-CTG CCC TGT GCT TGG CAC CTT GTA CAG CTC-3′. Insertion of EmGFP into the NCX3.2 cDNA between the aspartic acid (D^{37}) and valine (V^{38}) required another two fragments. One was from the N-terminal to D^{37} using the primers NCX3.2-start: 5′-GCC GCC ACC ATG GCG TGG TTA AGG TTG-3′ and SP + GFP-R: 5′-CTC GCC CTT GCT CAC CAT GTC CCC TGA GCC-3′. The other was from V^{38} to the C-terminal end of NCX3.2 using the primers GFP + NCX3-F: 5′-ATG GAC GAG CTG TAC AAG FTF CCA CGC ACA-3′ and NCX3-orf-end-R: 5′-GAA CCC CTT GAT GTA GCA ATA GGC-3′. Subsequently, using the three fragments as templates, the NCX3.2-EmGFP was constructed by PCR with the primers NCX3.2-start: 5′-GCC GCC ACC ATG GCG TGG TTA AGG TTG-3′ and NCX3-orf-end-R: 5′-GAA CCC CTT GAT GTA GCA ATA GGC-3′. The NCX3.2-EmGFP was cloned into the pcDNA3.1-NCX3.2/V5-His TOPO vector according to the method described in the previous study (Lindgren et al., 2005).

Site directed mutagenesis was carried out using a protocol based on the QuikChange® Site-Directed Mutagenesis Kit (Stratagene) using the plasmid (pcDNA3.1-NCX3.2/V5-His) with primers (mutated nucleotides are underlined) N45D-F: 5′- CAA GCA CAG GGC AGA ACG ATG AGT CCT GTT CAG GG-3′ and N45D-R: 5′- CCC TGA ACA GGA CTC ATC GTT CTG CCC TGT GCT TG-3′ for N45D mutation, and primers N67D-F: 5′-CAA TCT GGT ACC CGG AGG ACC CTT CCC TTG GGG AC-3′ and N67D-R: 5′-GTC CCC AAG GGA AGG GTC CTC CGG GTA CCA GAT TG-3′ for N67D mutation. In this way, the asparagine residues N45 and N67 in two putative *N*-linked glycosylation motifs of NCX3 (see Fig. 6D and F) were mutated to aspartic acid. The respective cDNA mutants and resulting proteins were designated as NCX3-N45D and NCX3-N67D. The introduced mutations were confirmed by sequencing.

2.3. RNA interference (RNAi) for gene silencing

Information on specific siRNAs used in this study is as follows: SLC8A3 Stealth Select RNAi™ siRNA (HSS143968), SLC8A3 Stealth Select RNAi™ siRNA (HSS143969) and SLC8A3 Stealth Select RNAi™ siRNA (HSS143970). The scrambled Stealth RNAi™ siRNA Negative Control Kit (12935-100) with similar GC content recommended by Invitrogen was used as control siRNA.

2.4. Measurement of $[Ca^{2+}]_i$ in HeLa cells using Fura-2

HeLa cells were cultured in 35 mm Petri dishes and transfected with plasmids as indicated in each experiment. After 24 h, cells were rinsed with Ca^{2+}-free Krebs buffer and loaded with 5 μM Fura-2/AM in 2 ml of the same buffer for 30 min at 37 °C in the dark. Subsequently, cells were rinsed with the buffer twice and the Petri dish was attached to a microscope stage and monitored with time-lapse microscopy. Measurements were carried out at 37 °C using a heat-controlled chamber (Warner Instruments) with a cooled electron-multiplying charged-coupled device Cascade II:512 camera (Photometrics) mounted on an inverted microscope (Carl Zeiss) equipped with a 25 × 0.8 NA. lens (Carl Zeiss). Excitation at 340 nm and 380 nm was assessed with a high-speed illumination system (DG-4, Sutter Instrument). MetaFluor (Molecular Devices) was used to control all devices and to analyze acquired images. Thapsigargin (1 μM) was added for releasing Ca^{2+} from ER into cytosol. The area under the curve was calculated to compare responses.

2.5. SDS-PAGE and Western blotting

Transfected cells were pelleted and dissolved in SDS-sample loading buffer (0.125 M Tris, 15% (v/v) glycerol, 5 mM EDTA, 2% SDS, 0.1% (w/v) bromophenol blue, 1% (v/v) 2-mercaptoethanol, pH6.8) prior to a 10 min incubation at 100 °C. Samples were separated on a 10% polyacrylamide gel, transferred to PVDF (Immobilon P, Millipore), and probed using a monoclonal anti-V5 antibody (1:5000, Thermo Fisher). Subsequently, the blots were incubated with an anti-mouse secondary antibody conjugated to horse-radish peroxidase (Amersham), and immunocomplexes were detected with enhanced chemiluminescence (ECL) (Amersham). In some experiments, transfected HEK293T cells were treated (at 12 h post-transfection) with and without tunicamycin (an inhibitor of *N*-linked glycosylation, Sigma) for an additional 20 h followed by immunoblotting analysis.

2.6. Indirect immunofluorescence

The HEK293T and HeLa cells were seeded onto glass coverslips after one day, transfected with plasmids, and were fixed (4%

paraformaldehyde in PBS, 15 min) at 24 h post-transfection. Cells were then incubated in blocking buffer (2% BSA in PBS buffer) followed by monoclonal anti-V5 antibody (1:500 in blocking buffer, 12–16 h, 4 °C). For co-staining with cell organelle markers, the cells were stained with different marker antibodies following the protocols provided by vendors. Cells were washed thoroughly in PBS prior to incubation with secondary antibody with color of fluorescence. After a final PBS wash, the coverslips were mounted with the Mounting Medium containing DAPI (Vector Laboratories). For endogenous NCX3 co-immunostaining with different cell organelle markers, the SH-SY5Y human neuroblastoma cells were seeded, fixed and stained as above. The NCX3 polyclonal antibody (SWANT) was used at 1:600 dilution in blocking buffer.

2.7. Live cell imaging

Leica TCS SP5 II confocal system (Leica) and INU2 incubation system for microscopes (TOKAI HIT) constituted the integrated live cell imaging system. 100% pure CO_2 was supplied by AGA and the CO_2 concentration 5% at 160 ml/min was automatically configured. HEK293T cells transfected with NCX3-EmGFP were cultured in 35 mm glass bottom Petri dishes (Mat Tek Corporation) for 24 h before imaging. The movie was made by Imaris (Bitplane).

2.8. BrdU incorporation

HEK293T cells growing on coverslips were transfected with plasmids, and cultured for 18 h. At the end of this period cells were incubated with BrdU (20 μM/ml) in media for another 4 h and then fixed in 1% paraformaldehyde in PBS buffer for 8 min, followed by 1% formalin, 0.3% Triton X-100 in PBS for 18 h at 4 °C. BrdU immunolabeling was performed with anti-BrdU mAb (Amersham). The immunoreaction was detected by incubation with secondary antibodies conjugated to Rhodamine. For analysis of BrdU incorporation in transfected cells, BrdU-labeled cultures were subsequently immunostained with anti-V5 pAb (Abcam) as described above.

2.9. Premo™ FUCCI Cell Cycle analysis

HEK293T cells were seeded on coverslips in 6-well plates one day before transfection. NCX3.2-V5 plasmid DNA was transduced into the cells on coverslips. After 4 h, the transfection medium was changed to 1 ml culture medium and subsequently we followed the protocol for fixation as recommended with the Premo™ FUCCI Cell Cycle Sensor (BacMam 2.0) (Invitrogen™) analysis kit.

2.10. FACS analysis

HEK293T cells transfected with different plasmids were trypsinized, resuspended in media, spun down for 5 min at 200 x g, washed twice in PBS, and fixed in 95% ethanol on ice for 5 min. While vortexing, cells were resuspended in 70% ethanol and left at 4 °C overnight before staining. Cells were stained at room temperature for 2–3 h in 50 μg/ml propidium iodide in PBS. Cells were analyzed on a FACSCalibur cell sorter using CellQuest software (Beckton Dickinson, Mountain View, CA), and the percentages of cells in the G0/G1, S, and G2/M phases of the cell cycle were determined using ModFit LT software (Verity Software House, Topsham, ME).

2.11. Antibodies and reagents

Mouse monoclonal antibodies (mAbs) used in this study were V5-tag (Invitrogen), Anti-Nucleoporin and Anti-GM130 (BD Biosciences), GAPDH and anti-EGFR (Santa Cruz). Rabbit polyclonal antibodies (pAbs) were anti-NCX3 (SWANT), V5-tag (Abcam) and anti-PDI (Cell signaling). Secondary antibodies included the DyLight 488- and 649-conjugated anti-mouse and anti-rabbit IgG antibodies (Vector Laboratories) for immunofluorescence and the peroxidase-conjugated anti-mouse and anti-rabbit IgG antibodies (Amersham) for immunoblotting. ER Staining Kit − Red Fluorescence Cytopainter (Abcam) and MitoTracker Red CMXRos (Thermo Fisher) for staining of ER and mitochondria were used.

2.12. Statistical analysis

The two-tailed unpaired *t*-test was applied to evaluate differences between experimental groups using GraphPad software. Error bars represent standard deviation of mean (SD). *p*-values less than or equal to 0.05 were considered as statistically significant.

3. Results

3.1. Subcellular localization of human NCX3

To better understand the physiological functions of human NCX3, we first investigated its subcellular localization. We previously constructed an expression plasmid containing a full-length human NCX3.2 (NM_182932.1, NCX3 isoform 2) with a C-terminal V5/His tag (pcDNA3.1-NCX3.2/V5-His) (Lindgren et al., 2005). Cells (HEK293T) were transiently transfected with this plasmid and were examined by immunofluorescence staining (Fig. 1A). We found that overexpression of NCX3 resulted in two main patterns of subcellular localization. The percentage of cells that showed NCX3 localized to the plasma membrane, a phenotype denoted NCX3-PM, was 44%, whereas 56% of the cells showed intracellular NCX3, predominantly associated with the nuclear envelope and the ER, a phenotype denoted NCX3-ER (Fig. 1A and B).

Double immunofluorescence analysis of HEK293T cells stably expressing NCX3 using a monoclonal antibody against PDI (protein disulfide isomerase) (Abcam) as the ER marker and anti-V5 polyclonal antibody for NCX3-V5 confirmed that the introduced NCX3 localized to the ER, as the two proteins showed a high degree of co-localization (Fig. 1C). To better dissect the sub-cellular distribution of NCX3, we used different cell organelle markers and performed co-staining with the exogenously expressed NCX3 in HEK293T and HeLa (Fig. 1D and E, Supplementary Figs. S1 and S2). We used the ER Staining Kit (Abcam) to confirm distribution in ER and a monoclonal antibody against nucleoporin as the nuclear envelope marker to study NCX3 perinuclear distribution. We confirmed that the NCX3 foci in cells with ER phenotype mainly co-localized with ER marker and Nucleoporin (Fig. 1D and E, Supplementary Fig. S2B and C). The monoclonal epidermal growth factor receptor (EGFR) antibody (Santa Cruz) was used as a plasma membrane marker. In HEK293T and HeLa expressing NCX3.2-V5, we noticed co-localization between NCX3 and EGFR foci, which was in accordance with a plasma membrane localization of the NCX3, especially in cells approaching the stage of mitosis (Fig. 1F). Considering a potential NCX3 subcellular localization in mitochondria and in the Golgi apparatus, Mitotracker (mitochondrial marker) and the monoclonal GM130 antibody (Golgi apparatus marker) were co-stained with exogenously expressed NCX3. Minor foci of NCX3 were found on mitochondria as well as overlapping with the Golgi apparatus in HEK293T cells (Supplementary Fig. S1A and B).

On the basis of these results, in HEK293T and HeLa cells expressing NCX3.2-V5, the main distribution of exogenously introduced NCX3 was defined as either in the nuclear envelope and ER (NCX3-ER phenotype), or in the plasma membrane (NCX3-PM phenotype). Furthermore, we could not rule out the potential localization of NCX3 in mitochondria and Golgi apparatus.

Experimentally introduced ectopic expression of plasmid DNA is under debate for its artificial effects compared with the endogenous protein function. The endogenous NCX3 proteins are specifically expressed in brain and skeletal muscle (Lindgren et al., 2005) and not

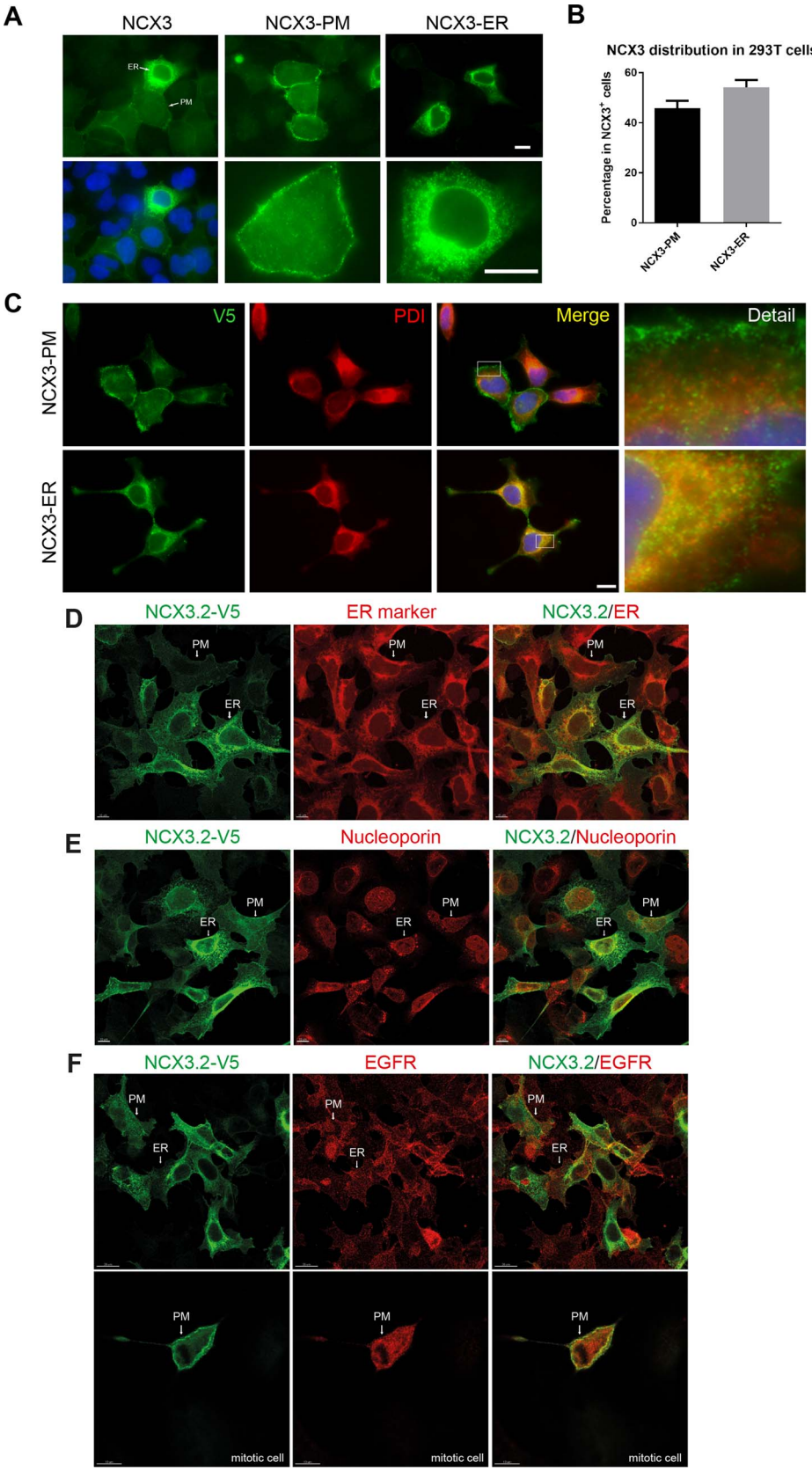

Fig. 1. Subcellular localization of exogenously introduced human NCX3.2-V5/His. HEK 293T cells were transiently transfected with NCX3 (NCX3.2-V5), resulting in two phenotypes of subcellular localization, denominated NCX3-PM and NCX3-ER (A). Quantitative analysis of NCX3-PM (44%) and NCX3-ER (56%) phenotypes of $NCX3^+$ cells. Three independent experiments were performed and 300 $NCX3^+$ cells were counted in each experiment (B). NCX3-V5 stably expressing HEK293T cells, showing co-localization of NCX3 (green) and the PDI ER marker (red) preferentially in NCX3-ER phenotype cells. Scale bars represent 20 μm (C). By confocal microscopy, co-localization of NCX3 with ER, nuclear envelope, and plasma membrane was analyzed in HEK293T cells transfected with NCX3.2-V5. NCX3 (green) in cells displayed NCX3-PM (arrow with PM) and NCX3-ER (arrow with ER) phenotypes. ER (red) was stained with ER Staining Kit – Red Fluorescence – Cytopainter (Abcam) and mainly co-localized with green fluorescence in NCX3-ER phenotype cells. Scale bars represent 10 μm (D). Nuclear envelope was stained with anti-nucleoporin antibody (red) and mainly co-localized in the NCX3-ER phenotype cells. Scale bars represent 10 μm (E). Plasma membrane was stained with anti-EGFR antibody (red) and mainly co-localized in the NCX3-PM phenotype cells (upper images). Cells in mitosis showed stronger NCX3-PM green foci and co-localization with plasma membrane EGFR marker (red) (lower images). Scale bars represent 10 μm (F). (For interpretation of the references to colour in this figure legend, the reader is referred to the web version of this article.)

normally present in HEK293T cells. To confirm the NCX3-PM and NCX3-ER localization phenotypes endogenously in cells, we identified a specific polyclonal NCX3 antibody and human cells with abundant expression of the NCX3 protein. The specific NCX3 antibody was validated by knockdown of NCX3 expression in SH-SY5Y (neuroblastoma), U-343MG, and U-343MGa Cl2:6 (glioma) cells using 3 pairs of NCX3 siRNAs (Fig. 2A). SH-SY5Y cells were found to express a relatively high NCX3 protein level, whereas NCX3 was undetected

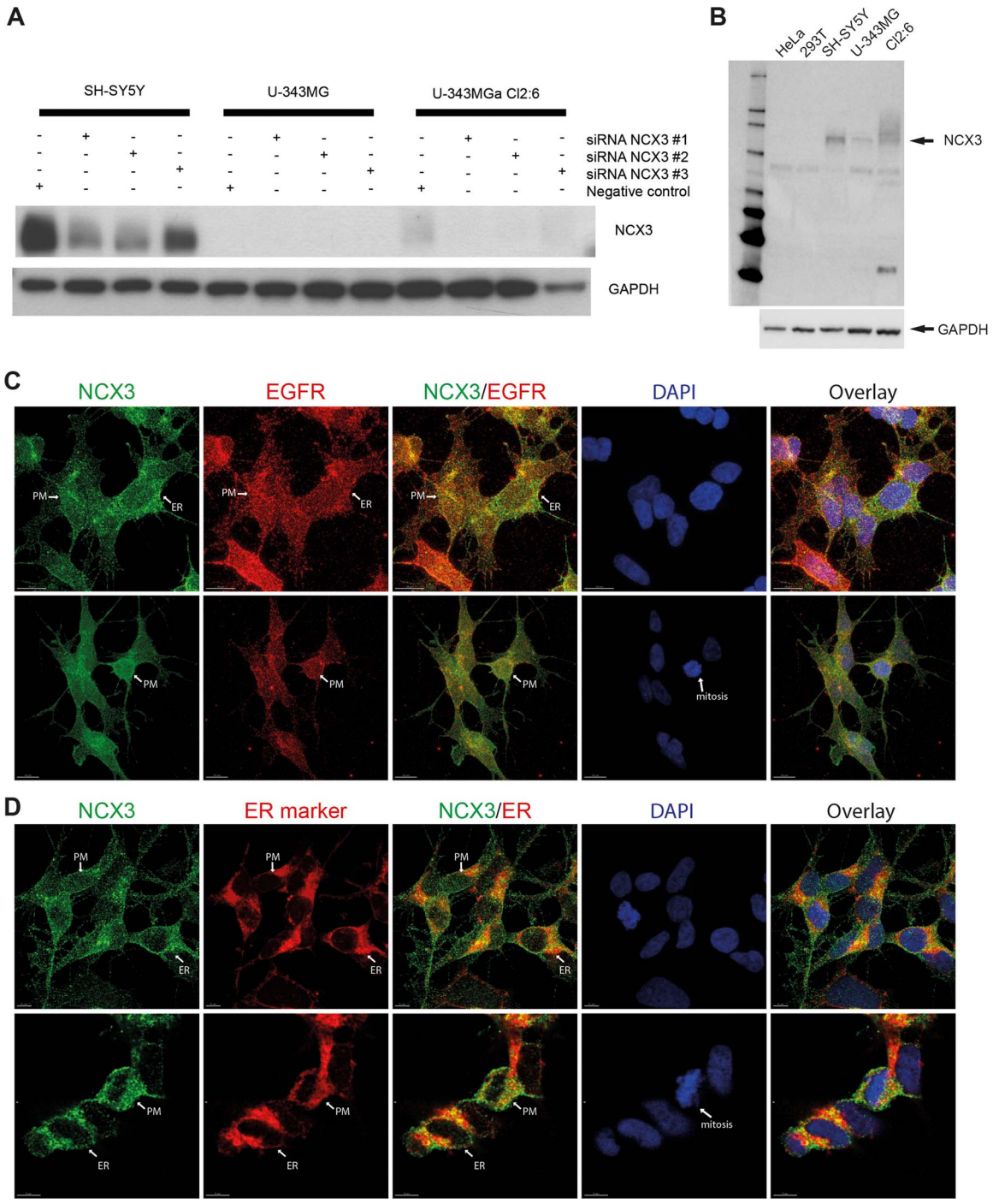

Fig. 2. Subcellular localization of endogenous NCX3 in SH-SY5Y cells. Validation of a specific NCX3 antibody was done by knockdown of NCX3 with siRNAs. Three pairs of NCX3 siRNAs and scrambled Stealth siRNA were introduced into SH-SY5Y, U-343MG, and U-343MGa Cl2:6 cells. The NCX3 protein is more abundant in SH-SY5Y cells than that in U-343MGa Cl2:6 cells, and #1 and #2 siNCX3 s worked efficiently in these cells. The NCX3 antibody (Swant) was diluted 1:6000 in blocking buffer for immunoblotting (A). Endogenous NCX3 expression levels in different cell lines. NCX3 was expressed in SH-SY5Y (lane 3) and U-343MGa Cl2:6 (lane 5) but not in HeLa (lane 1) and HEK 293T cells (lane 2). The NCX3 antibody generates the most specific signal in SH-SY5Y cells without obvious extra bands (lane 3) The lower band in U-343MG (lane 4) is unspecific to the NCX3 protein. (B). Confocal microscopy visualized co-localization of NCX3 with plasma membrane (PM) and endoplasmic reticulum (ER) in SH-SY5Y cells. NCX3 (green) distribution indicated NCX3-PM (arrow with PM) and NCX3-ER (arrow with ER) phenotypes. Plasma membrane was stained with anti-EGFR antibody (red) and this mainly co-localized with NCX3 in the NCX3-PM phenotype cells (upper images). Cells in mitosis showed stronger NCX3-PM green foci and co-localization with plasma membrane marker EGFR (red) (lower images) (C). ER (red) was stained with ER Staining Kit – Red Fluorescence – Cytopainter (Abcam) and the signal mainly co-localized with NCX3 in the NCX3-ER phenotype cells. The cells in mitosis showed stronger NCX3-PM green foci and less co-localization with ER marker (red) relative to NCX3-ER phenotype (lower images). (D). Scale bars represent 10 μm. (For interpretation of the references to colour in this figure legend, the reader is referred to the web version of this article.)

endogenously in HEK293T and HeLa cells (Fig. 2A and B). The antibody recognized NCX3 most specifically in SH-SY5Y cells, without marked extra bands (Fig. 2B). By co-staining of NCX3 both with the anti-EGFR antibody and the ER marker, we found that the NCX3-ER phenotype (green foci) co-localized less with EGFR (red foci) (Fig. 2C), but more with the ER-marker (Fig. 2D) as compared with the NCX3-PM phenotype in SH-SY5Y cells. Furthermore, the NCX3-PM distribution seemed more dominant when the cell was in mitosis (Fig. 2C and D). These

patterns were in line with the results obtained in HEK293T and HeLa cells exogenously expressing NCX3.2-V5, although more delicate.

Accordingly, we selected the HEK293T and HeLa cells with exogenously expressed NCX3.2-V5 for further functional experiments in this study because the endogenous NCX3 protein was not very abundant even in SH-SY5Y cells. Furthermore, SH-SY5Y cells showed a high intercellular variation, which would be disturbing in functional studies as well as in further subcellular localization analysis.

3.2. The effect of NCX3 on intracellular Ca^{2+} transients

It is generally accepted that NCXs function as plasma membrane antiporters regulating intracellular Ca^{2+} homeostasis. We therefore examined if/how the two NCX3 distribution phenotypes described above could affect the cells' Ca^{2+} handling when exogenously expressed in HeLa cells. NCX3 transfected cells were detected by co-transfecting a GFP plasmid and the result was compared to cells transfected with the GFP plasmid alone. The cytosolic Ca^{2+} concentration was measured by loading cells with Fura-2/AM and performing time-lapse ratiometric Ca^{2+} imaging. To deplete the ER of Ca^{2+}, cells were challenged with 1 μM Thapsigargin (Tg, SERCA pump inhibitor) in the absence of extracellular Ca^{2+}. When the cytosolic Ca^{2+} level decayed back to base line, the recording solution was exchanged to Ca^{2+}-containing media plus 1 μM Tg to allow capacitative Ca^{2+} entry. Using this experimental approach, Tg and external Ca^{2+} readdition elicited Ca^{2+} responses in cells (Fig. 3A) and in cells expressing exogenous NCX3 (Fig. 3B). Although resting Ca^{2+} levels were similar under both conditions (Fig. 3D), quantitative analysis indicated that overexpressed NCX3 dramatically decreased the ER-Ca^{2+} release capacity, as the total Ca^{2+} released upon Tg stimulation (Fig. 3C), the transient increase upon Tg stimulation (Fig. 3E), and the transient increase upon Ca^{2+} readdition (Fig. 3F) were significantly decreased in cells overexpressing NCX3 compared to control cells.

3.3. Cells in which NCX3 was predominantly localized to the ER were not actively proliferating

When observing the subcellular distribution of NCX3, we noticed that very few cells with NCX3-ER distribution were in mitosis, in contrast to cells with the NCX3-PM phenotype. This observation suggested that the subcellular localization of NCX3 could be cell cycle-dependent or even regulate cell cycle progression. Thus, we used a BrdU incorporation assay to determine the fraction of cells in S phase. Cells (HEK293T) were transfected with the NCX3-expression vector (NCX3.2-V5) or the GFP-expression control vector only. Eighteen hours post-transfection, BrdU was added to the media and cells were fixed after 4 h incubation followed by double immunofluorescence staining using anti-BrdU mouse monoclonal antibody and anti-V5 polyclonal antibodies (for NCX3). $BrdU^+$ cells were quantitated in the two cell populations displaying the different NCX3 phenotypes. Representative immunofluorescence images are shown in Fig. 4A. Three independent experiments were performed and 100 $BrdU^+$ cells were counted in each experiment. Quantitative analysis revealed that the percentage of $BrdU^+$ cells was lower in cells with NCX3-ER phenotype (5.1%) than in control cells (44.7%). Conversely, the number of $BrdU^+$ cells was higher in cells with NCX3-PM phenotype (62%) than in control cells (Fig. 4B).

NCX3.2-V5 was further expressed in HeLa cells and its sub-cellular distribution detected by immunofluorescence staining. Cell nuclei were stained with DAPI (Supplementary Fig. S3). We found the NCX3-ER phenotype in interphase cells, whereas the NCX3-PM phenotype was dramatically increased in mitotic cells and in cells undergoing division. Importantly, in mitotic cells, NCX3 was predominantly localized in plasma membrane.

To further verify the hypothesis that the subcellular distribution of NCX3 varied with cell cycle phase, we measured the percentages of NCX3-PM and NCX3-ER phenotypes in S/G2/Mitosis phases using the fluorescence ubiquitination cell cycle indicator (Premo FUCCI Cell Cycle Sensor) system (Sakaue-Sawano et al., 2008). HEK293T cells seeded on the coverslips were transfected with 2 μg NCX3.2-V5 plasmid DNA in 6-well plates. After 4 h, the transfection medium was changed to 1 ml culture medium in each well and Premo reagents (geminin-GFP and Cdt1-RFP) were added in a total volume of 40 μl. The cells were incubated overnight, then fixed with paraformaldehyde, immunostained with anti-V5 antibody and secondary DyLight 649 conjugated anti-mouse antibody and analyzed with confocal microscopy. Examples of the stained cells are shown (Fig. 4C). Geminin-GFP^+ cells

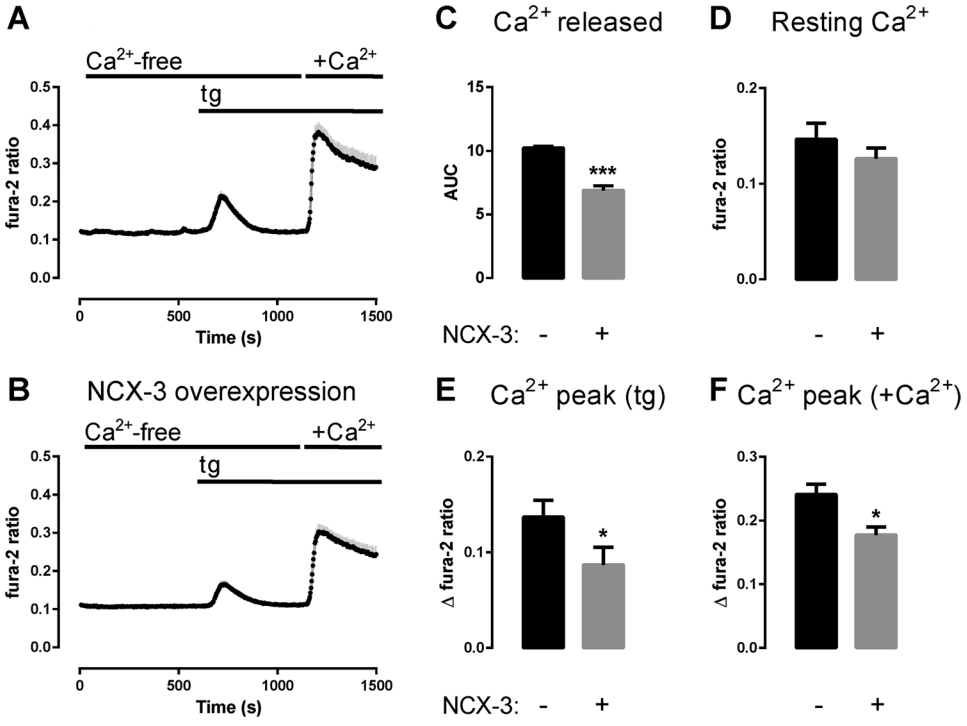

Fig. 3. The effect of NCX3 on intracellular Ca^{2+} transients in HeLa cells. The co-expression of NCX3 and GFP vector in the same HeLa cell defined NCX3 overexpressing cells, "NCX3 overexpression" cells (M = 46, N = 3). The expression of EmGFP vector only in HeLa cells defined control cells (M = 40, N = 3). Three independent experiments were performed (N = 3) and M represents the number of cells analyzed in all three independent experiments. Fura-2 pre-loaded cells were analyzed by time-lapse ratiometric Ca^{2+} imaging (340/380 nm excitation ratio for fura-2). Tg (1 μM) and external Ca^{2+} readdition elicited Ca^{2+} response in control cells (A) and NCX3 overexpressing cells (B). The total Ca^{2+} released upon Tg stimulation was dramatically decreased in NCX3 overexpressing cells. Area under the curve (AUC) stands for ER-Ca^{2+} release capacity (C), while the resting Ca^{2+} levels were similar in the two conditions (D). The transient amplitude upon Tg addition was significantly decreased in NCX3 overexpressing cells (E), as was the transient amplitude upon Ca^{2+} readdition (F). (Values represent the average of three different experiments ± S.D; * means p-value ≤ 0.05; *** means p-value ≤ 0.001.).

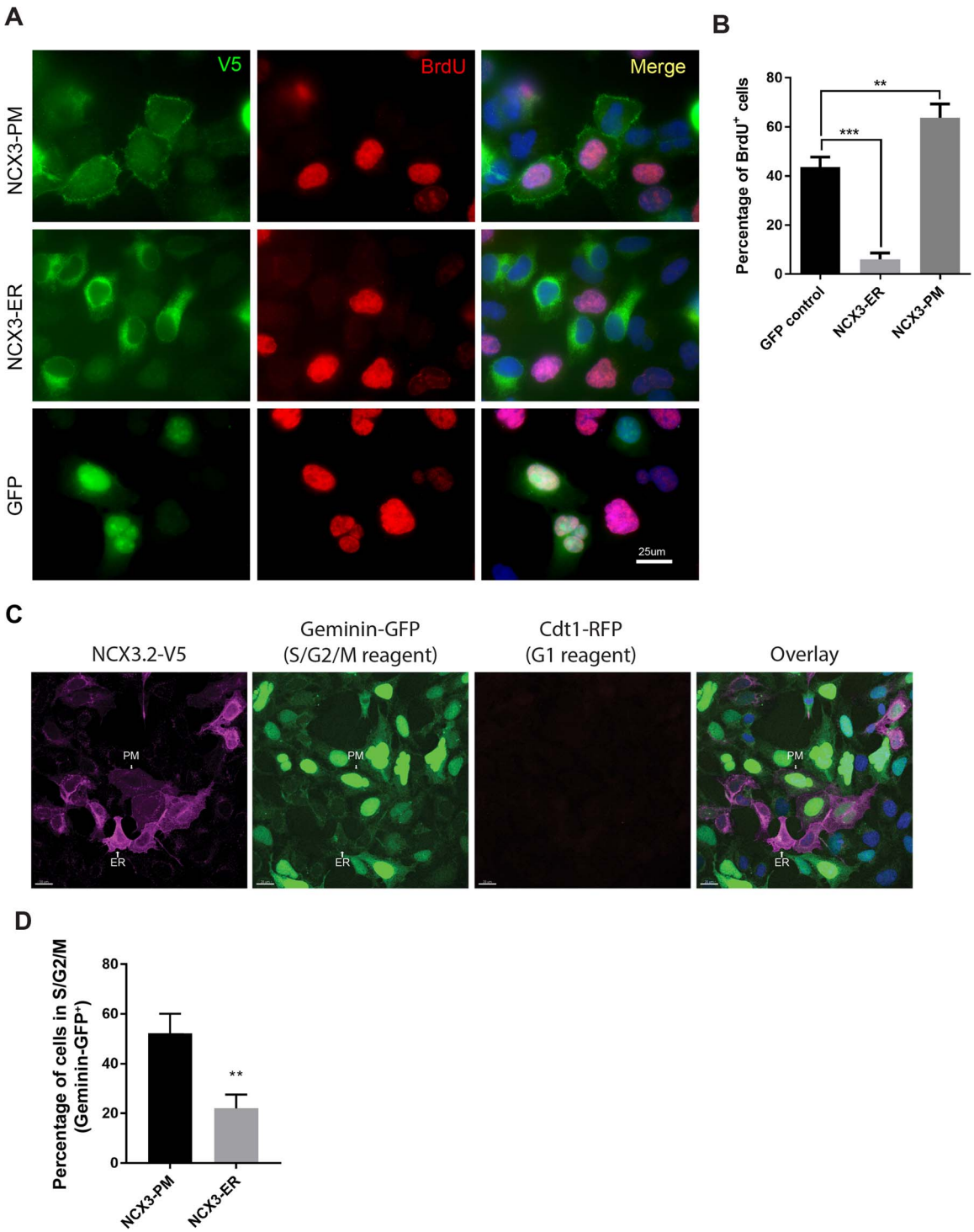

Fig. 4. BrdU incorporation (DNA synthesis) assay in HEK 293T cells with NCX3 overexpression (A, B) and subcellular localization of NCX3 in HEK293T cells during different cell cycle phases (C, D). NCX3-PM and NCX3-ER phenotype cells incorporate BrdU at different levels. Cultures transfected with GFP vector only were monitored as a control (A). Quantitative analysis of the percentage $BrdU^+$ cells in GFP control, NCX3-ER and NCX3-PM cells. Three independent experiments were performed and 100 $BrdU^+$ cells were counted in each experiment. Error bars represent standard deviation of mean (SD). (** means p-value ≤ 0.01 (here $p = 0.0075$); *** means p-value ≤ 0.001 (here $p = 0.0002$)) (B). Premo™ FUCCI Cell Cycle analysis in HEK 293T cells expressing NCX3.2. NCX3 protein (magenta) showed NCX3-PM and NCX3-ER subcellular distribution. The cells expressing geminin-GFP displayed green foci in nuclei which marks cells in S/G2/M phases. The Cdt1-GFP (red) positive nuclei marks the cells in G1 phase(C). Geminin-GFP+ cells were quantitated in the two cell populations displaying the different NCX3 phenotypes. Three independent experiments were performed and 60 cells with NCX3-PM phenotype and 60 cells with NCX3-ER phenotype were counted in each experiment. Within the counted NCX3-PM and NCX3-ER populations, the geminin-GFP+ cells (cells in S/G2/M phases) were counted for further analysis. Quantitative analysis revealed that the percentage of geminin-GFP+ cells was lower (~22%) in cells displaying NCX3-ER phenotype than the percentage (~52%) in cells with NCX3-PM distribution. Error bars represent standard deviation of mean (SD). (** means p-value ≤ 0.01 (here $p = 0.0022$)). (For interpretation of the references to colour in this figure legend, the reader is referred to the web version of this article.)

were quantitated in the two cell sub-populations displaying the different NCX3 phenotypes. Three independent experiments were performed and 60 cells of each phenotype were counted in each experiment. Within the counted NCX3-PM and NCX3-ER populations, the geminin-GFP$^+$ cells (cells in S/G2/M phases) were counted for further analysis. Quantitative analysis revealed that the percentage of geminin-GFP$^+$ cells was lower in cells displaying the NCX3-ER phenotype (~22%) than in cells with the NCX3-PM phenotype (~52%) ($p < 0.01$) (Fig. 4D). This finding indicated that the cells with the NCX3-PM phenotype were more abundant in S/G2/M phases and more prone to proliferation than the cells with NCX3-ER phenotype. This was consistent with the BrdU incorporation assay results.

In summary, all these data demonstrated that the NCX3-ER phenotype predominates in interphase cells that are not actively synthesizing DNA or undergoing cell division, whereas the NCX3-PM phenotype is seen in cells undergoing DNA synthesis, mitosis, and cell division. Thus, the process that normally controls NCX3 subcellular distribution is dynamic and linked to the cells' choice between arrest and progression through the cell cycle.

3.4. Tracking the dynamics of NCX3 subcellular distribution by live cell imaging

It was exciting to see that the subcellular distribution of NCX3 varied with the cell cycle. To further illustrate these variations, we constructed an NCX3 recombinant with GFP (EmGFP). In this new construct, the EmGFP peptide was inserted into the region of mature NCX3.2, between the aspartic acid (D^{37}) and valine (V^{38}), which is in the region following the signal peptide and in front of a putative *N*-glycosylation site. The construct subcloned into the pcDNA3.1-NCX3.2/V5-His vector, was denoted as NCX3-EmGFP-V5 (Fig. 5A). A band of ~125 kDa was detected by immunoblotting using anti-V5 monoclonal antibody in HEK293T cells transiently expressing the construct. The molecular mass increased by ~30 kDa, compared with that of NCX3-V5, which corresponds to the expected EmGFP molecular mass (Fig. 5B).

Next, we performed live cell imaging to analyze NCX3 dynamics in real time. Cells (HEK293T) were cultured in 35 mm glass bottom Petri dishes (MatTek) and transfected with NCX3-EmGFP-V5. After 24 h we monitored the dynamic subcellular distribution of NCX3 for 18 h using a Leica TCS SP5 II confocal system (Fig. 5C, Supplementary Fig. S4). In cells approaching mitosis, NCX3 accumulated in the plasma membrane gradually. When cells had entered mitosis, NCX3 was mostly located in the plasma membrane, i.e. displayed the NCX3-PM phenotype. Also during telophase, the NCX3-PM phenotype was maintained and when reaching cytokinesis, the phenotype changed moderately from NCX3-PM to NCX3-ER. In the two daughter cells, NCX3-ER was the predominant phenotype (Fig. 5C). The entire time-lapse series visualizing the dynamic NCX3 subcellular distribution is presented as supplementary information (Fig. S4 movie). In summary, this experiment demonstrated that NCX3 subcellular distribution is a dynamic process in synchrony with the cell cycle. These data support the findings presented in Fig. 4B, showing that a majority of cells with the NCX3-ER phenotype had not incorporated BrdU (did not synthesize DNA).

3.5. Human NCX3 protein is post-translationally modified by N-glycosylation

To better understand the underlying mechanisms regulating the differential subcellular distribution of NCX3 we studied its biochemical properties. To this end, NCX3 was transiently expressed in HEK293T cells and the cell lysate was subjected to Western blot analysis. The NCX3-V5 vector generated a doublet band of ~100–93 kDa (Fig. 6A). Presumably, the doublet band at 100 kDa could be due to post-translational modification.

Based on the above finding, we asked ourselves if post-translational modification was associated with the differential subcellular distribution of NCX3. To unravel this question, the nuclear fraction (including partial ER fraction as the nuclear envelope is associated with the ER in the cell) was isolated from HEK293T cells transiently expressing NCX3 and subjected to immunoblotting analysis. We found that the nuclear fraction did not contain the higher molecular weight species at ~100 kDa, but only the lower molecular weight species at ~93 kDa (Fig. 6B). These results implied that post-translational modification might be associated with the differential subcellular distribution of NCX3.

A previous study (Hryshko et al., 1993) reported the presence of *N*-linked glycosylation in the cardiac Na^+/Ca^{2+} exchanger (NCX1). We therefore assumed that the same post-translational modification could occur in NCX3 as well. To address this question, HEK293T cells transiently expressing NCX3-V5 were grown in the presence and absence of tunicamycin (an inhibitor of *N*-glycosylation), and cell lysates were subjected to immunoblotting analysis. As shown in Fig. 6C, upon treatment with tunicamycin the upper band at ~100 kDa disappeared (lanes 3 and 4), and only the lower molecular weight band at ~93 kDa remained when compared with lysates from cells not treated with tunicamycin (lanes 1 and 2). This indicated that the upper band represented an *N*-glycosylated form, and the lower band a non-glycosylated form of the exchanger. Taken together, these experiments indicate that human NCX3 is glycosylated via *N*-linked glycosylation and that both *N*-glycosylated and non-glycosylated forms of NCX3 can be present in HEK293T cells.

3.6. N-glycosylation is important for targeting of NCX3 to the plasma membrane

Fig. 6D (upper) presents the putative molecular structure of the human NCX3 protein based on hydropathy analysis of the amino acid sequence (Gabellini et al., 2002). Initial bioinformatics analysis of the human NCX3 amino acid sequence predicted that there were two potential *N*-glycosylation sites in the N-terminal extracellular region (Fig. 6D, lower). To see if the two potential *N*-glycosylation sites were present not only in the NCX3.2 isoform precursor but also in other reported human full-length NCX3 isoforms, we queried The Basic Local Alignment Search Tool (BLAST) analysis system with the NCX3.2 isoform protein sequence (NP_891977.1) and collected other reported full-length NCX3 precursors using the Constraint-based Multiple Alignment Tool (COBALT) for multiple protein sequence alignment (Altschul et al., 1997; Papadopoulos and Agarwala, 2007). We found that different NCX3 isoforms have the same N-terminal sequence including the two predicted *N*-glycosylation sites (Fig. 6F). Accordingly, we postulate that findings made in the present study on the NCX3.2 isoform can be applied broadly to other full-length NCX3 isoforms.

In an effort to verify the two potential *N*-linked glycosylation sites, we separately mutated the asparagine residues 45 and 67 in the two putative *N*-linked glycosylation motifs of NCX3 to aspartic acid (designated as NCX3-N45D and NCX3-N67D). Mutant proteins were expressed in HEK293T cells by transient transfection and characterized by Western blot analysis. We found that the two mutant NCX3 proteins were different in their gel migration patterns as detected by Western blotting. The NCX3-N45D mutation resulted in a shift of the higher molecular weight band (~100 kDa) to the lower molecular weight band (~93 kDa), while the NCX3-N67D mutant migrated similar to the wild-type NCX3-V5 and thus, the latter mutation did not affect the protein molecular weight in transfected cells. This demonstrated that *N*-linked glycosylation primarily occurred in asparagine residue 45 but not in residue 67 (Fig. 6E).

We next investigated the effect of *N*-glycosylation on the subcellular distribution of NCX3. The wild-type and the mutant forms of NCX3 were transiently expressed in HEK293T cells, and their subcellular distribution was investigated by immunofluorescence analysis. Representative examples are shown in Fig. 7A, in which it is evident

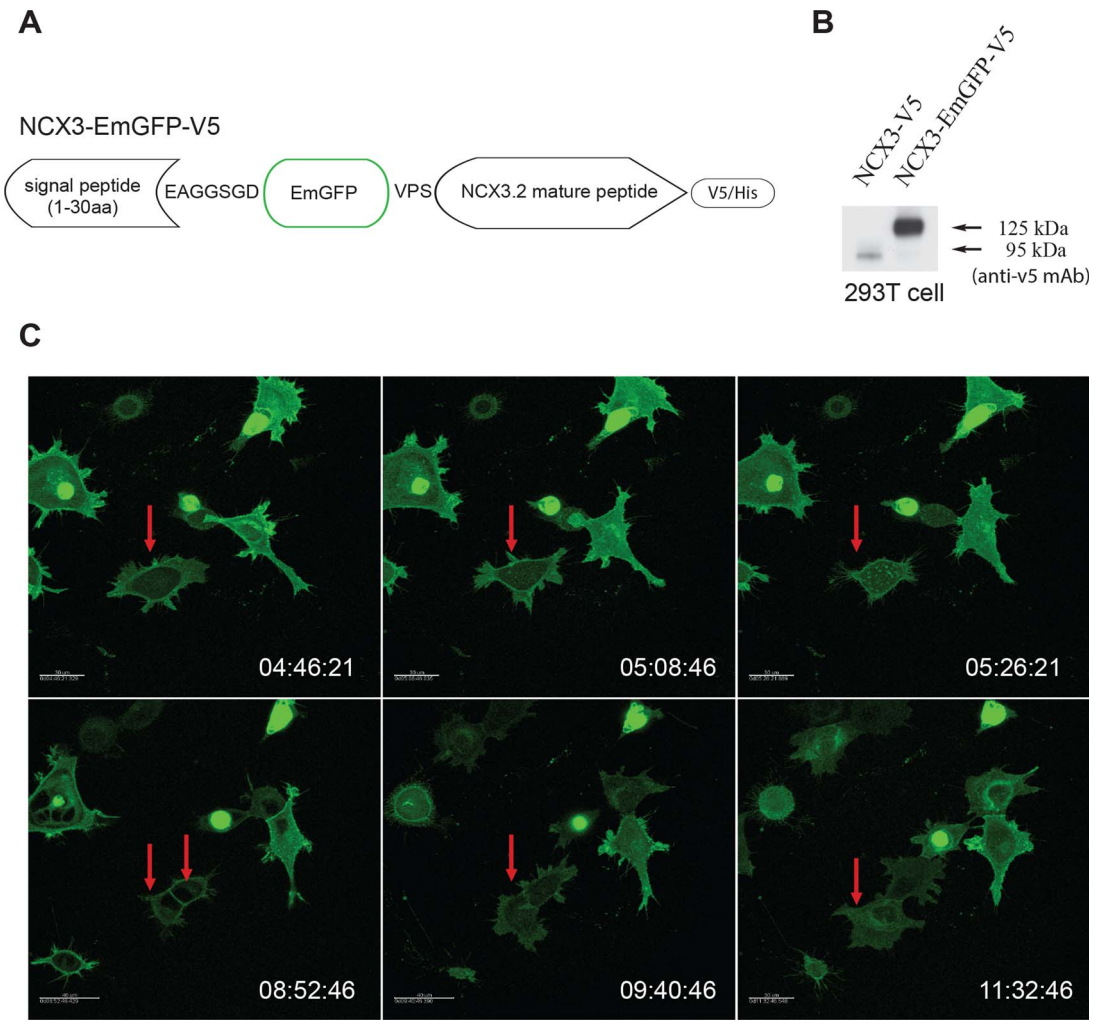

Fig. 5. NCX3-EmGFP-V5 construct and dynamic changes of its subcellular distribution during cell division. NCX3-EmGFP fusion recombinant was constructed. The EmGFP sequence was inserted in the amino-terminal part of NCX3 in-between the D^{37} and V^{38} amino acids (A). Western blot analysis of NCX3-V5 and NCX3-EmGFP-V5 overexpressed in HEK293T cells (B). Snapshots of NCX3-EmGFP subcellular localization in 293T cells from a time course of live cell imaging. Scale bar represents 10 μm (C). For the live cell imaging movie, see Supplementary Fig. S4.

that the *N*-glycosylation-deficient mutant (NCX3-N45D) is predominantly restrained in the cytosol (ER). However, the subcellular distribution of the wild-type and the NCX3-N67D mutant proteins was similar, and both the two cell phenotypes NCX3-PM and NCX3-ER were present in the NCX3-N67D transfected HEK293T cultures. These results showed that *N*-glycosylation at amino acid N45 but not at N67 is required for targeting of NCX3 to the plasma membrane.

The NCX3-N45D mutant was also evaluated regarding effects on intracellular Ca^{2+} transients in HeLa cells, using the same experimental setup as shown in Fig. 3, and making sure that only the NCX3 mutant and control transfected cells, respectively were measured in the different cultures. Cells overexpressing NCX3-N45D (Fig. 7C) responded similar as cells overexpressing wild-type NCX3 (Fig. 3B) when exposed to Tg or Ca^{2+} readdition. Overexpressing NCX3-N45D largely attenuated total Ca^{2+} released from ER (Fig. 7D), as well as the Ca^{2+} released by Tg (Fig. 7F), and the effect of Ca^{2+} readdition (Fig. 7G), whereas resting Ca^{2+} levels were not significantly changed. These results indicate that the glycosylation-deficient form of NCX3, which is accumulated in the ER, is functional and can actively pump Ca^{2+} from the cytosol into the ER (forward mode). In summary, we noted that WT and glycosylation deficient NCX3 had similar effects in that both of them strikingly decreased Ca^{2+} transients when overexpressed in cells.

3.7. The N-glycosylation-deficient mutant NCX3-N45D causes accumulation of cells in the G0/G1 phase of the cell cycle

Taken together, the results suggest that the NCX3-ER phenotype represents a non-glycosylated form of the NCX3 protein localized in the ER. We further studied if the *N*-glycosylation-deficient mutant NCX3-N45D, which was restrained in the ER had any effect on cell cycle distribution. Cells (HEK293T) transiently transfected with plasmids containing either the wild-type NCX3 or the NCX3-N45D mutant were harvested 24 h post-transfection and analyzed by FACS. Indeed, cell cultures that expressed the NCX3-N45D mutant showed an increased percentage of cells in the G0/G1 phase (60.3%) compared with cultures expressing wild-type NCX3 (51.5%). Consistent with this, the percentage of cells in S phase was decreased (Fig. 8). Three independent FACS experiments using cultures with high transfection efficiencies (~60%) were performed with similar results, supporting the hypothesis that the *N*-glycosylation-deficient mutant NCX3-N45D which is stalled in the ER, delays cells in the G0/G1 phase of the cell cycle, preventing cells from proliferating. A possible interpretation of this finding is that since the mutant NCX3 protein is restrained in the ER, it can continue to actively pump Ca^{2+} from the cytosol into the ER and this would potentially attenuate the intracellular Ca^{2+} transients.

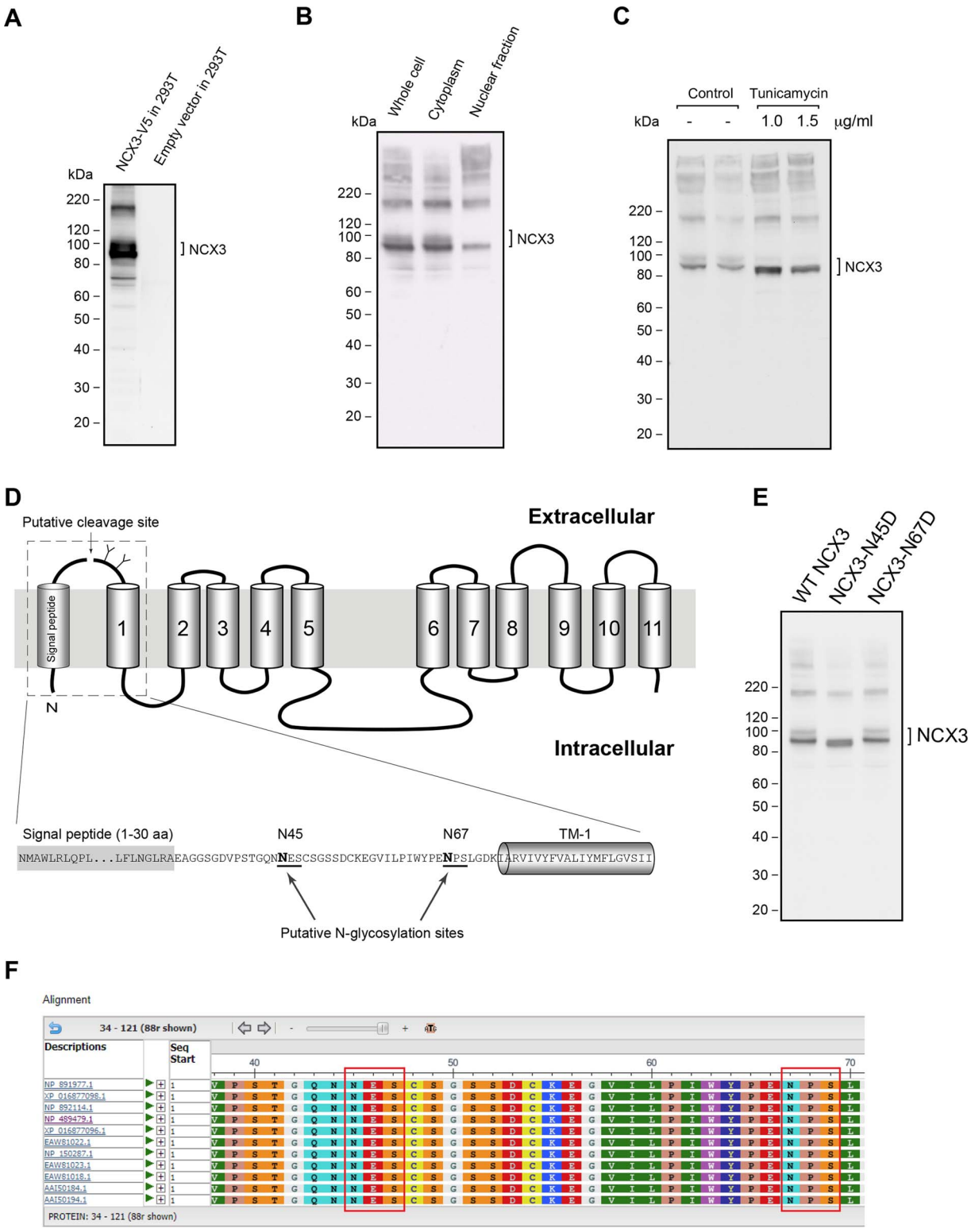

Fig. 6. Biochemical characterization of human NCX3 protein and its post-translational modification by *N*-glycosylation. The different NCX3 constructs were expressed in HEK293T cells. Western blot analysis shows a doublet band for NCX3.2-V5 overexpressed in HEK293T cells (A). The nuclear fraction contains only the lower molecular weight species of NCX3 (B). NCX3 is post-translationally modified by *N*-glycosylation. Tunicamycin treatment for 3 h decreased the higher molecular weight species of NCX3 (C). Domain structure of NCX3 (upper). Amino acid sequence from the signal peptide to the first transmembrane domain (TM-1) in the N-terminal region of human NCX3. The two potential *N*-glycosylation sites (consensus *N*-glycosylation motif, NXT/S, X = any amino acid) are underlined with the asparagine residue (N) in bold (lower) (D). *N*-glycosylation properties of human NCX3 protein *N*-glycosylation site mutants, NCX3.2-N45D and NCX3.2-N67D shown by Western blot analysis (E). Multiple alignment of the protein sequences in NCX3 full-length precursors with COBALT tool.

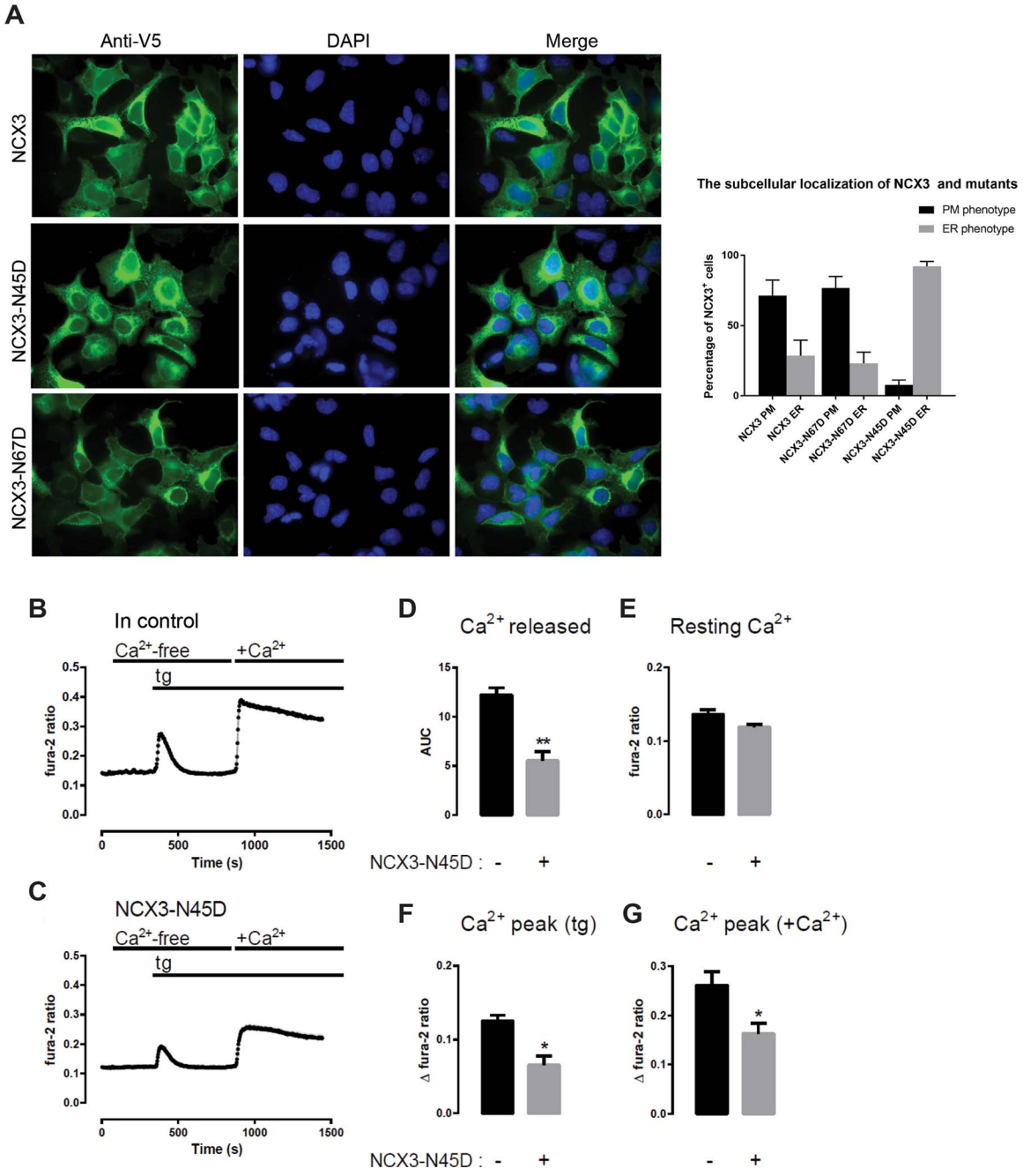

Fig. 7. The subcellular localization of human NCX3 *N*-glycosylation site mutants (A) and the effect of NCX3-N45D on intracellular Ca^{2+} transients compared to GFP transfected control cells (B-G). Comparison of NCX3, NCX3-N45D and NCX3-N67D subcellular localization in 293T cells. Similar to NCX3 wildtype, NCX3-PM and NCX3-ER phenotypes were detected in NCX3-N67D expressing HEK293T cells. In contrast, only the NCX3-ER phenotype could be found in HEK293T cells expressing NCX3-N45D. Immunofluorescence staining (left) and percentages of NCX3-PM and NCX3-ER phenotype cells in the different transfected cultures as indicated (right). Three independent experiments were performed and 30 GFP^+ transfected cells were counted in each experiment (A). The co-expression of NCX3-N45D and GFP vector in HeLa cells was used to identify the cells with exogenous expression of NCX3 N45D (M = 49, N = 3), in live cell imaging. The expression of GFP vector only in HeLa cells identified as control cells (M = 39, N = 3). Three independent experiments were performed (N = 3) and M represents the number of cells analyzed in all three independent experiments. Fura-2 pre-loaded cells were analyzed by time-lapse ratiometric Ca^{2+} imaging (340/380 nm excitation ratio for fura-2). Tg (1 μM) and external Ca^{2+} readdition elicited Ca^{2+} response in control cells (B) and in NCX3-N45D overexpressing cells (C). Area under the curve (AUC) stands for ER-Ca^{2+} release capacity. The total Ca^{2+} released upon Tg stimulation was dramatically decreased in NCX3-N45D overexpressing cells compared to the control cells (D). The resting Ca^{2+} levels were similar in the two conditions (E) while the transient amplitude upon Tg stimulation was significantly decreased in NCX3-N45D overexpressing cells (F), as was the transient amplitude upon Ca^{2+} readdition (G). (Values represent the average of three different experiments ± S.D; * means *p*-value ≤ 0.05; ** means *p*-value ≤ 0.01.).

4. Discussion

Changes in the intracellular Ca^{2+} concentration are dynamic and versatile mechanisms that control a plethora of cellular processes (Berridge et al., 2000). Plasma membrane and intracellular channels, pumps, buffers and exchangers can in concert achieve a complex and tight regulation of Ca^{2+} homeostasis. The NCXs are transport proteins of high capacity. They were traditionally regarded as mainly responsible for influx/efflux of Ca^{2+} across the plasma membrane, but differences in their tissue and subcellular distribution indicate distinct functions in cellular physiology.

It is well known that the NCX family members are targeting the plasma membrane. However, in the rat central nervous system, NCX3 is scattered within the cytoplasm and also linked to plasma membrane,

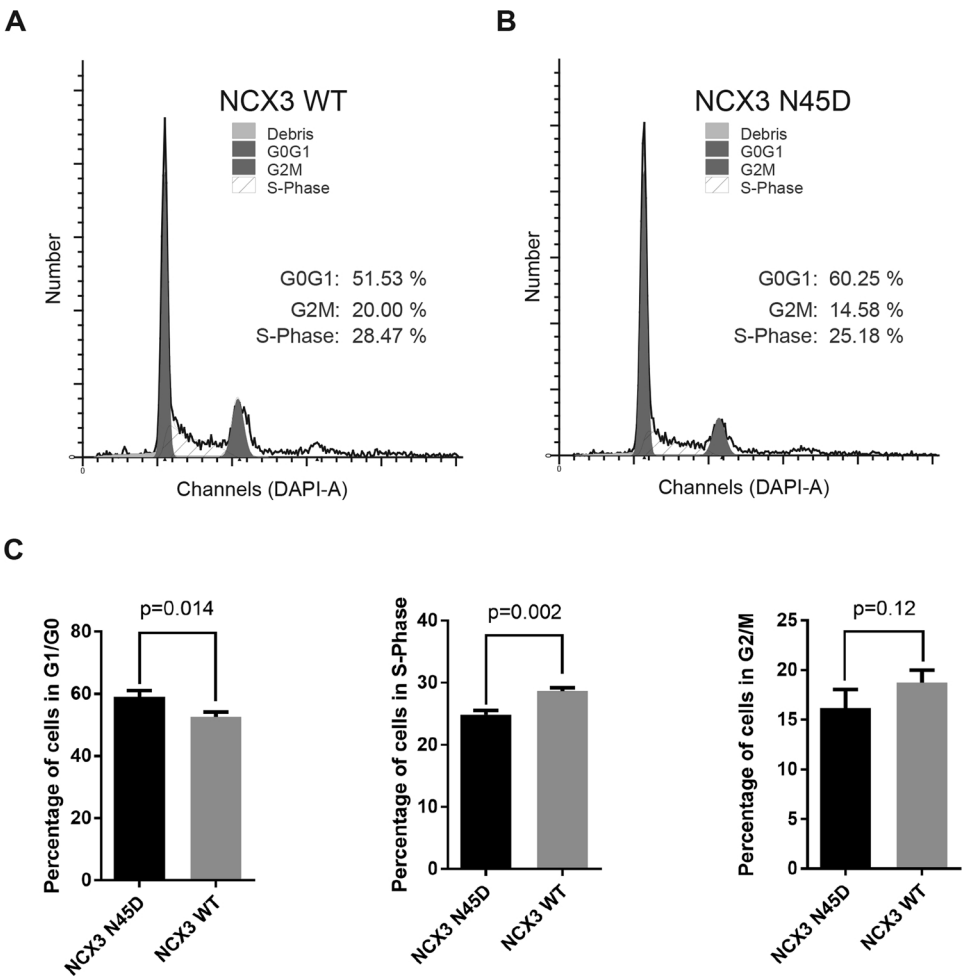

Fig. 8. FACS analysis to monitor the effect of the NCX3 *N*-glycosylation-deficient mutant (NCX3-N45D) on cell cycle progression. HEK293T cells were transiently transfected with either wild-type NCX3 (NCX3.2-WT) (A) or the *N*-glycosylation-deficient mutant (NCX3-N45D) (B). DNA content was measured by FACS analysis. Each experiment was repeated three times and one representative experiment is shown in A-B. There was a significant increase in the percentage of cells in the G0/G1 phase of the cell cycle in all tested cell populations expressing NCX3.2-N45D protein ($p < 0.02$), with concomitant decreases in the percentages of S phase cells ($p = 0.002$) compared with control cells expressing wild-type NCX3 (NCX3.2-WT). There was a trend but no significant difference in G2/M phase cells ($p = 0.12$). Statistical analysis was performed on the basis of three representative experiments using the two-tailed unpaired *t*-test (C).

perinuclear cisterns and mitochondria (Minelli et al., 2007). In addition, there are several more recent studies indicating that NCX(3) can promote uptake of Ca^{2+} in both ER and mitochondria (Hampton et al., 2000; Laskowski and Medler, 2009; Scorziello et al., 2013). In the present study, we demonstrate that exogenous expression of human NCX3 simultaneously produces two dominant subcellular distribution phenotypes, NCX3-PM and NCX3-ER, in HEK293T cells. The BrdU incorporation assay and live cell imaging unraveled a potential correlation between the two phenotypes and progression or not through the cell cycle. Only 5.1% of cells with the NCX3-ER phenotype incorporated BrdU, while in comparison 62% of cells with the NCX3-PM phenotype and 44% of GFP-expressing control cells incorporated BrdU. Thus, when NCX3 was confined to the cytosol, that is in the ER (and in NE), most of the cells seemed not to be actively synthesizing DNA. However, when localized to the plasma membrane, NCX3 seemingly promoted cell cycle progression, at least when compared with GFP-expressing control cells.

Exogenous expression of fluorescent NCX3-EmGFP-V5 in HEK293T cells facilitated tracking the subcellular dynamics of NCX3 by live cell imaging. The distribution of the NCX3 protein varied in cells and, most importantly, these variations were synchronized with the cells' resting vs. progression through the cell cycle. By using the Premo™ FUCCI Cell Cycle analysis tool it could be additionally confirmed that in S-phase, mitosis, and cell division stages, NCX3 is a plasma membrane protein, while resting/interphase cells, mainly displayed the NCX3-ER phenotype. Cytosolic Ca^{2+} plays a critical role in cell proliferation and apoptosis (Berridge et al., 2000), and there is a general agreement that Ca^{2+} signaling is implicated and altered during cell cycle progression (Whitaker and Larman, 2001; Whitaker, 2006). Our findings that, in S-phase, mitosis, and cell division stages, NCX3 is almost entirely accumulated in the plasma membrane are in line with previous findings, whereas the finding that NCX3 is confined to the ER of resting interphase cells is more intriguing. One way of interpreting these findings would be that in interphase cells the role of NCX3 is to clear any cytoplasmic overload by transporting Ca^{2+} into the ER. By live cell imaging, we also observed that when cells prepared for mitoses their plasma membrane movements increased, and the NCX3-PM signal was most intense at the edge of the forming membrane ruffles. We speculate that in preparation for a new round of the cell cycle, the ER-PM phenotype may participate in generating the initial, transient cytosolic Ca^{2+} peaks induced for example by growth factor receptor signaling (Soliven, 2001; Butt, 2006; Boscia et al., 2012) and generated by influx of Ca^{2+} through the plasma membrane (Khananshvili, 2014; Kortus et al., 2016), while NCX3-ER might promote the subsequent Ca^{2+} decline by acting in the refilling of Ca^{2+} into ER (Davis et al., 2009; Pannaccione et al., 2012; Michel et al., 2015).

The notion of an association between growth factor signaling and activation of the NCX3 protein is further strengthened by the phenotype of NCX3-null mice (Boscia et al., 2012). Characteristics of these mice are defective oligodendrocyte progenitor cell (OPC) differentiation, defective myelination, and smaller brains. OPC proliferation and differentiation is known to be regulated by PDGF-AA and PDGF-AA may be coupled to micro-domains on oligodendrocyte processes harboring NCX3 (Boscia et al., 2012; Khananshvili, 2014).

In the excellent paper by Javier Garcia-Sancho (Garcia-Sancho, 2014), it is described how chromaffin cells (neuroendocrine cell type) harbour sub-plasmalemmal high Ca^{2+} concentration micro-domains (HCMD) from which Ca^{2+} is taken up into sub-plasmalemmal

mitochondria. In contrast, in non-excitable cells exemplified by HEK293 cells the Ca^{2+} concentration in the respective HCMD is much lower and Ca^{2+} is taken up by ER rather than by mitochondria and further released to the cytoplasm via NCX. Mitochondria are normally "empty" and can transiently accumulate large amounts of Ca^{2+} when needed, whereas ER intracellular stores normally are filled and can release Ca^{2+} to enforce local Ca^{2+} signals. Thus, that paper suggests that NCX is localized in mitochondria of the chromaffin cells, and that HEK293T cells instead primarily takes up Ca^{2+} in ER. Our findings indicate the possibility that the attenuation of the Ca^{2+} signal occurs via NCX3 positioned in the ER of HEK293T cells, and HeLa cells, since the measurements were done in those cells. The abovementioned paper also discusses other mechanisms of Ca^{2+} attenuation in ER than via NCX (privileged coupling between SOCE and SERCA in non-excitable cells).

Glycosylation is a common modification of proteins that enter the ER. Some proteins require *N*-linked glycosylation for proper folding in the ER and for targeting to their destinations in the cell. In this work, Western blotting identified a doublet band at about 100/93 kDa representing the exogenously expressed NCX3.2 protein. In consistence with the two phenotypes observed, we detected the 93 kDa band but not the 100 kDa band in the nuclear fraction (with perinuclear membranes) isolated from HEK293T cells transiently overexpressing NCX3. The endogenous NCX3 protein bands visualized by immunoblotting in SH-SY5Y cells also showed the typically indistinct "smear" of differentially/partially glycosylated proteins. Furthermore, Tunicamycin inhibited formation of the 100 kDa protein band, thus inhibited glycosylation of the NCX3 WT protein. Subsequently the NCX3-N45D mutation experiment proved the 45th amino acid residue, asparagine to be a functional glycosylation site. This site seems to function as an on/off switch for the transportation of NCX3 protein to either be maintained in the cytosol (ER) or transported to the plasma membrane. Importantly, both the NCX3 WT and the glycosylation-deficient NCX3-N45D proteins were capable of pumping Ca^{2+} from the cytosol to the ER lumen as they were positioned in ER. Accordingly, both proteins functioned to attenuate the cytosolic Ca^{2+} upon ER Ca^{2+} release. Thus, a dynamic control of the NCX3 subcellular distribution and thereby its Ca^{2+} transport property may facilitate the fine-tuning of Ca^{2+} signaling and contribute to the regulation of cell cycle progression and cell proliferation. From this also follows that the dynamic change of NCX3 subcellular distribution would be required to promote cell proliferation as is shown in the present work. Overexpressing wild-type NCX3 with its dominating ER phenotype and overexpressing the glycosylation deficient NCX3 mutant that is stalled in ER resulted in similar effects: decrease of cytoplasmic Ca^{2+} transients and inhibition of cell cycle progression.

To confirm that the NCX3-PM and -ER phenotypes are present endogenously in cells and not only artifacts of ectopically expressed NCX3, we performed cell organelle co-localization studies of endogenous NCX3 in neuroblastoma cells in parallel with the overexpressing HEK293T and HeLa cells, since these cells displayed detectable endogenous levels of the protein. The presence of preferential −PM versus −ER/perinuclear NCX3 distribution in different cells of the neuroblastoma culture was confirmed. A minor distribution of NCX3 in mitochondria and Golgi apparatus was also observed.

The dynamics of NCX3 subcellular distribution and the involvement of the glycosylation site, N^{45}, introduce a new perspective on how the cell can direct the trafficking of NCX3 to different subcellular compartments. A variety of modifications exist in protein biosynthesis. Since glycosylation of NCX3 facilitates translocation of the protein to the plasma membrane, it is reasonable to think that other modifications could promote the translocation of NCXs to various organelles and cellular compartments, depending on physiological requirements. In the case of endogenous NCXs, as the protein level is low, it has previously been difficult to detect any apparent intracellular foci of the protein by immunofluorescence microscopy. It is reasonable to assume that the fine-tuned subcellular dynamics of endogenous NCXs and their delicate functions therefore have remained undetected in normal cells in many instances. Here, by using neuroblastoma cells and a specific polyclonal NCX3 antibody we managed to visualize such foci.

In this context, it is important to note that all here analyzed full-length NCX3 splice variants are conserved in the N-terminal region surrounding the N45 glycosylation site, whereas this site is not conserved in NCX1 and 2, although other potential *N*-glycosylation sites were predicted in the similar area of NCX1 and 2 protein sequence (Supplementary Fig. S5B). Furthermore, in a bioinformatics search of NCX3 domains, potential *N*-glycosylation sites, and sequence variants, the different mutations reproted in cancer cells/samples were found to be relatively equally distributed over the whole length of the NCX3 protein (Supplementary Fig. S5A). Worth noting is the fact that no cancer mutations have yet been reported in a short segment covering the NCX3 N45 glycosylation site investigated here. If anything, this can be taken as an indication of its crucial function in cell life (Supplementary Fig. S5A).

A recent review (Giladi et al., 2016) deals primarily with the fine-tuned regulation of exchanger activity, the importance of physical interactions between CBD1 and CBD2, their regulatory Ca^{2+} and Na^{+} binding capacity and secondary local allosteric modifications affecting the exchanger activity in quite complex ways. Regulation involves especially the differentially spliced region in CBD2, affecting the exchanger activity once it has been integrated in the plasma membrane or in other intracellular organelles. On the other hand, these mechanisms are said not to affect trafficking of the NCX molecule. One important point of the present work is that the N45 glycosylation site is located in the far N-terminal end of the NCX3 protein, and is specifically shown to affect trafficking and sub-cellular localization of the protein. When the WT and glycosylation deficient (N45 site mutant) proteins were overexpressed in HeLa cells they seemed to have similar effects on intracellular processing of Ca^{2+} (and uptake into ER), indicating that even if lack of *N*-glycosylation affects subcellular trafficking and prevents the full-length exchanger from reaching the cell membrane this does not necessarily the exchangers Ca^{2+} transport activity once integrated in the ER membrane.

Thus, much of the detailed functional regulation of the Na^{+}/Ca^{2+} exchanger proteins NCX1-3 is still confined to the large hydrophilic intracellular loop. However, no potential *N*-glycosylation site was identified in this region of NCX1-3. Interestingly, one conserved putative *N*-glycosylation site (NVT) was identified in the C-terminal half of all the three NCX proteins. This was predicted to be present in an extracellular position in the C-terminal region between the 8th and 9th transmembrane segments (see Supplementary Fig. S5B).

One important point here is that the N45 glycosylation site is unique to NCX3 and conserved in all aligned NCX3 splice isoform sequences (Fig. 6F and Supplemental information). The N45 glycosylation site is not conserved in NCX1 and 2, but other N-glycolysation sites were predicted at NCX1 N44 and NCX2 N34 (supplemental information). For comparison, we have aligned NCX3 with NCX1 and NCX2 full-length sequences and also aligned the mitochondrial antiporter NCLX.

Finally, the NCLX, a long-sought mitochondrial NCX protein, which is the single mammalian member of a phylogenetically ancestral branch of the NCX superfamily, has been characterized by others. The alignment of its amino acid sequence illustrates that NCLX is quite divergent from the NCX1-3 proteins (Supplementary Fig. S5B).

Conflict of interest

The authors declare no conflict of interest.

Acknowledgments

This work was supported by grants from the Swedish Research Council (VR-NT; VR-MH; VR-Linné STARGET) and from the Swedish

Cancer Society, the Cancer Society in Stockholm, Karolinska Institutet and the Stockholm County Council. It was also supported by grants from the Swedish Research Council (grant 2013-3189 to P.U.); the Swedish Brain Foundation (grant FO2015-0074 to P.U.) and the Swedish Cancer Society (grant CAN 2016-801 to P.U.).

Appendix A. Supplementary data

Supplementary data associated with this article can be found, in the online version, at https://doi.org/10.1016/j.ejcb.2018.02.004.

References

Altschul, S.F., Madden, T.L., Schaffer, A.A., Zhang, J., Zhang, Z., Miller, W., Lipman, D.J., 1997. Gapped BLAST and PSI-BLAST: a new generation of protein database search programs. Nucleic Acids Res. 25, 3389–3402.

Berridge, M.J., Lipp, P., Bootman, M.D., 2000. The versatility and universality of calcium signalling. Nat. Rev. Mol. Cell Biol. 1, 11–21.

Boscia, F., D'Avanzo, C., Pannaccione, A., Secondo, A., Casamassa, A., Formisano, L., Guida, N., Sokolow, S., Herchuelz, A., Annunziato, L., 2012. Silencing or knocking out the Na+/Ca2+ exchanger-3 (NCX3) impairs oligodendrocyte differentiation. Cell Death Differ. 19, 562–572.

Brini, M., Carafoli, E., 2011. The plasma membrane Ca(2)+ ATPase and the plasma membrane sodium calcium exchanger cooperate in the regulation of cell calcium. Cold Spring Harb. Perspect. Biol. 3, a004168.

Butt, A.M., 2006. Neurotransmitter-mediated calcium signalling in oligodendrocyte physiology and pathology. Glia 54, 666–675.

Davis, K.A., Samson, S.E., Hammel, K.E., Kiss, L., Fulop, F., Grover, A.K., 2009. Functional linkage of Na+-Ca2+-exchanger to sarco/endoplasmic reticulum Ca2+ pump in coronary artery: comparison of smooth muscle and endothelial cells. J. Cell. Mol. Med. 13, 1775–1783.

Gabellini, N., Bortoluzzi, S., Danieli, G.A., Carafoli, E., 2002. The human SLC8A3 gene and the tissue-specific Na+/Ca2+ exchanger 3 isoforms. Gene 298, 1–7.

Garcia-Sancho, J., 2014. The coupling of plasma membrane calcium entry to calcium uptake by endoplasmic reticulum and mitochondria. J. Physiol. 592, 261–268.

Giladi, M., Khananshvili, D., 2013. Molecular determinants of allosteric regulation in NCX proteins. Adv. Exp. Med. Biol. 961, 35–48.

Giladi, M., Tal, I., Khananshvili, D., 2016. Structural features of ion transport and allosteric regulation in sodium-calcium exchanger (NCX) proteins. Front. Physiol. 7, 30.

Hampton, T.G., Wang, J.F., DeAngelis, J., Amende, I., Philipson, K.D., Morgan, J.P., 2000. Enhanced gene expression of Na+/Ca2+ exchanger attenuates ischemic and hypoxic contractile dysfunction. Am. J. Physiol. Heart Circul. Physiol. 279, H2846–2854.

Hilge, M., Aelen, J., Vuister, G.W., 2006. Ca2+ regulation in the Na+/Ca2+ exchanger involves two markedly different Ca2+ sensors. Mol. Cell 22, 15–25.

Hryshko, L.V., Nicoll, D.A., Weiss, J.N., Philipson, K.D., 1993. Biosynthesis and initial processing of the cardiac sarcolemmal Na+-Ca2+ exchanger. Biochim. Biophys. Acta 1151, 35–42.

Iwamoto, T., Shigekawa, M., 1998. Differential inhibition of Na+/Ca2+ exchanger isoforms by divalent cations and isothiourea derivative. Am. J. Physiol. 275, C423–430.

Iwamoto, T., Nakamura, T.Y., Pan, Y., Uehara, A., Imanaga, I., Shigekawa, M., 1999. Unique topology of the internal repeats in the cardiac Na+/Ca2+ exchanger. FEBS Lett. 446, 264–268.

Iwamoto, T., 2007. Na+/Ca2+ exchange as a drug target–insights from molecular pharmacology and genetic engineering. Ann N. Y. Acad. Sci. 1099, 516–528.

Khananshvili, D., 2014. Sodium-calcium exchangers (NCX): molecular hallmarks underlying the tissue-specific and systemic functions. Pflugers Arch. 466, 43–60.

Kortus, S., Srinivasan, C., Forostyak, O., Zapotocky, M., Ueta, Y., Sykova, E., Chvatal, A., Verkhratsky, A., Dayanithi, G., 2016. Sodium-calcium exchanger and R-type Ca(2+) channels mediate spontaneous [Ca(2+)]i oscillations in magnocellular neurones of the rat supraoptic nucleus. Cell Calcium 59, 289–298.

Laskowski, A.I., Medler, K.F., 2009. Sodium-calcium exchangers contribute to the regulation of cytosolic calcium levels in mouse taste cells. J. Physiol. 587, 4077–4089.

Lazniewska, J., Weiss, N., 2017. Glycosylation of voltage-gated calcium channels in health and disease. Biochim. Biophys. Acta 1859, 662–668.

Li, Z., Matsuoka, S., Hryshko, L.V., Nicoll, D.A., Bersohn, M.M., Burke, E.P., Lifton, R.P., Philipson, K.D., 1994. Cloning of the NCX2 isoform of the plasma membrane Na+-Ca2+ exchanger. J. Biol. Chem. 269, 17434–17439.

Liao, J., Li, H., Zeng, W., Sauer, D.B., Belmares, R., Jiang, Y., 2012. Structural insight into the ion-exchange mechanism of the sodium/calcium exchanger. Science 335, 686–690.

Linck, B., Qiu, Z., He, Z., Tong, Q., Hilgemann, D.W., Philipson, K.D., 1998. Functional comparison of the three isoforms of the Na+/Ca2+ exchanger (NCX1, NCX2, NCX3). Am. J. Physiol. 274, C415–423.

Lindgren, R.M., Zhao, J., Heller, S., Berglind, H., Nister, M., 2005. Molecular cloning and characterization of two novel truncated isoforms of human Na+/Ca2+ exchanger 3, expressed in fetal brain. Gene 348, 143–155.

Matsuoka, S., Nicoll, D.A., Reilly, R.F., Hilgemann, D.W., Philipson, K.D., 1993. Initial localization of regulatory regions of the cardiac sarcolemmal Na+-Ca2+ exchanger. Proc. Natl. Acad. Sci. U. S. A. 90, 3870–3874.

Michel, L.Y., Hoenderop, J.G., Bindels, R.J., 2015. Towards understanding the role of the Na+-Ca2+ exchanger isoform 3. Rev. Physiol. Biochem. Pharmacol. 168, 31–57.

Michel, L.Y.M., Verkaart, S., Latta, F., Hoenderop, J.G., Bindels, R.J., 2017. Differential regulation of the Na+-Ca2+ exchanger 3 (NCX3) by protein kinase PKC and PKA. Cell Calcium 65, 52–62.

Minelli, A., Castaldo, P., Gobbi, P., Salucci, S., Magi, S., Amoroso, S., 2007. Cellular and subcellular localization of Na+-Ca2+ exchanger protein isoforms, NCX1, NCX2, and NCX3 in cerebral cortex and hippocampus of adult rat. Cell Calcium 41, 221–234.

Moremen, K.W., Tiemeyer, M., Nairn, A.V., 2012. Vertebrate protein glycosylation: diversity, synthesis and function. Nat. Rev. Mol. Cell Biol. 13, 448–462.

Nicoll, D.A., Longoni, S., Philipson, K.D., 1990. Molecular cloning and functional expression of the cardiac sarcolemmal Na+-Ca2+ exchanger. Science 250, 562–565.

Nicoll, D.A., Quednau, B.D., Qui, Z., Xia, Y.R., Lusis, A.J., Philipson, K.D., 1996. Cloning of a third mammalian Na+-Ca2+ exchanger, NCX3. J. Biol. Chem. 271, 24914–24921.

Nicoll, D.A., Ottolia, M., Lu, L., Lu, Y., Philipson, K.D., 1999. A new topological model of the cardiac sarcolemmal Na+-Ca2+ exchanger. J. Biol. Chem. 274, 910–917.

Pannaccione, A., Secondo, A., Molinaro, P., D'Avanzo, C., Cantile, M., Esposito, A., Boscia, F., Scorziello, A., Sirabella, R., Sokolow, S., Herchuelz, A., Di Renzo, G., Annunziato, L., 2012. A new concept: abeta1-42 generates a hyperfunctional proteolytic NCX3 fragment that delays caspase-12 activation and neuronal death. J. Neurosci. 32, 10609–10617.

Papadopoulos, J.S., Agarwala, R., 2007. COBALT: constraint-based alignment tool for multiple protein sequences. Bioinformatics 23, 1073–1079.

Sakaue-Sawano, A., Kurokawa, H., Morimura, T., Hanyu, A., Hama, H., Osawa, H., Kashiwagi, S., Fukami, K., Miyata, T., Miyoshi, H., Imamura, T., Ogawa, M., Masai, H., Miyawaki, A., 2008. Visualizing spatiotemporal dynamics of multicellular cell-cycle progression. Cell 132, 487–498.

Schwarz, E.M., Benzer, S., 1997. Calx, a Na-Ca exchanger gene of Drosophila melanogaster. Proc. Natl. Acad. Sci. U. S. A. 94, 10249–10254.

Scorziello, A., Savoia, C., Sisalli, M.J., Adornetto, A., Secondo, A., Boscia, F., Esposito, A., Polishchuk, E.V., Polishchuk, R.S., Molinaro, P., Carlucci, A., Lignitto, L., Di Renzo, G., Feliciello, A., Annunziato, L., 2013. NCX3 regulates mitochondrial Ca2+ handling through the AKAP121-anchored signaling complex and prevents hypoxia-induced neuronal death. J. Cell. Sci. 126, 5566–5577.

Soliven, B., 2001. Calcium signalling in cells of oligodendroglial lineage. Microsc. Res. Tech. 52, 672–679.

Uhlen, P., Fritz, N., 2010. Biochemistry of calcium oscillations. Biochem. Biophys. Res. Commun. 396, 28–32.

Whitaker, M., Larman, M.G., 2001. Calcium and mitosis. Semin. Cell Dev. Biol. 12, 53–58.

Whitaker, M., 2006. Calcium microdomains and cell cycle control. Cell Calcium 40, 585–592.

Wu, G., Xie, X., Lu, Z.H., Ledeen, R.W., 2009. Sodium-calcium exchanger complexed with GM1 ganglioside in nuclear membrane transfers calcium from nucleoplasm to endoplasmic reticulum. Proc. Natl. Acad. Sci. U. S. A. 106, 10829–10834.

Xie, X., Wu, G., Lu, Z.H., Ledeen, R.W., 2002. Potentiation of a sodium-calcium exchanger in the nuclear envelope by nuclear GM1 ganglioside. J. Neurochem. 81, 1185–1195.